

## LECTURE 9

### Statistical mechanics of semiflexible polymers: theory and experiment\*

Erwin Frey, Klaus Kroy, Jan Wilhelm and Erich Sackmann

*Institut für Theoretische Physik und Institut für Biophysik,  
Physik-Department der Technischen Universität München,  
James-Franck-Straße, D-85747 Garching, Germany*

---

#### 1 Introduction and overview

Living cells are soft bodies of a characteristic form, but endowed with a capacity for a steady turnover of their structures. Both of these material properties, i.e. recovery of the shape after an external stress has been imposed and dynamic structural reorganization, are essential for many cellular phenomena. Examples are active intracellular transport, cell growth and division, and directed movement of cells. The structural element responsible for the extraordinary mechanical and dynamical properties of eukaryotic cells is a three-dimensional assembly of protein fibers, the *cytoskeleton*. A major contribution to its mechanical properties is due to actin filaments and proteins that crosslink them. Numerous experiments *in vivo* (Eichinger et al., 1996) and *in vitro* (Janmey, 1991; Janmey, 1995) have shown that the mechanical properties of cells are largely determined by the cytoskeletal network.

The cytoskeletal polymers (actin filaments, microtubules and intermediate filaments) which build up this network are at the relevant length-scales (a few microns at most) all *semiflexible polymers*. In contrast to flexible polymers the *persistence length* of these polymers is of the same order of magnitude as their total contour length. Hence, the statistical mechanics of such macromolecules can not be understood from the conformational entropy alone but depends crucially on the bending stiffness of the filament.

---

\*To be published in “Dynamical networks in physics and biology” (Proceedings of a Les-Houches workshop), edited by G. Forgacs and D. Beysens, EDP Sciences Springer Verlag (1998).

The nontrivial elastic response and distribution function of the end-to-end distance of a single semiflexible polymer illustrate instructively this interplay of energetic and entropic contributions. Fig. 1 shows the extension (in units of  $fL^2/k_B T$ ) of a semiflexible polymer of fixed length  $L$  grafted at one end when a weak force  $f$  is applied at the other end for different persistence lengths  $\ell_p$  (Kroy and Frey, 1996). This is one of the few *exact* results for the wormlike chain model. Note that the largest response is obtained for a polymer with a persistence length of the order of its contour length. More flexible molecules contract due to the larger entropy of crumpled conformations, stiffer molecules straighten out to keep their bending energy low. In the flexible case the response is isotropic and proportional to  $1/k_B T$ , i.e., the Hookian force coefficient is proportional to the temperature and we recover ordinary rubber elasticity. On the other hand, when the persistence length is longer than the contour length, the response becomes increasingly *anisotropic*. Transverse forces give rise to mechanical bending of the filaments and the transverse spring coefficient in the stiff limit is proportional to the bending modulus  $\kappa$ . The effective longitudinal spring coefficient turns out to be proportional to  $\kappa^2/T$ , indicating the breakdown of linear response at low temperatures  $T \rightarrow 0$  (or  $\ell_p \rightarrow \infty$ ). This is a consequence of the well known Euler buckling instability illustrated in Fig. 1 (top). The anisotropy of the elastic response considerably complicates the construction of network models.

Energetic effects also have a strong influence on the probability distribution function  $G(R; L)$  for the end-to-end distance  $R$  of a semiflexible polymer of length  $L$ . When the polymer is not much longer than its persistence length,  $G(R; L)$  deviates strongly from the Gaussian shape found for flexible polymers (see Fig. 2) with the main weight being shifted towards full extension with increasing stiffness (Wilhelm and Frey, 1996). This is also reflected by the nonlinear force-extension relation, whose overall shape is determined by the Euler instability. Measurements of the radial distribution function as well as of the response of single polymers to applied forces can be used to measure the bending stiffness of biopolymers.

A useful experimental technique for investigating the short time dynamics of semiflexible polymers is dynamic light scattering (Farge and Maggs, 1993; Harnau et al., 1996; Kroy and Frey, 1997). We have calculated the dynamic structure factor for solutions of semiflexible polymers in the weakly bending rod limit. The result allows characteristic parameters of the polymers, such as their persistence length  $\ell_p$ , their lateral diameter  $a$  and also the mesh size  $\xi_m$  of the network to be determined from light scattering measurements. The most important result of this work is that the decay of the dynamic structure factor shows two regimes, an initial simple exponential decay determined by the hydrodynamics of the solvent and a stretched exponential decay due to structural relaxation driven by the bending energy. For actin and intermediate filaments, where both regimes can be resolved, the

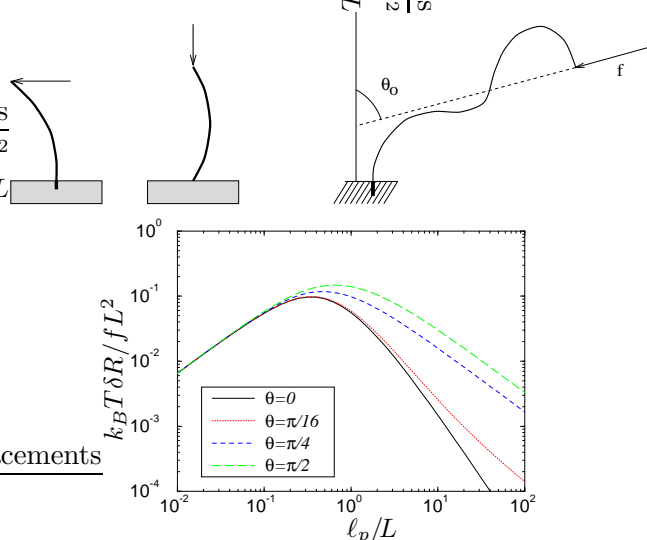


Figure 1: *Top:* The elastic response of a stiff rod is extremely anisotropic due to the Euler instability. *Bottom:* Response of a filament clamped at one end with a fixed initial orientation to a small external force at the other end. The normalized extension (inverse force coefficient) is plotted versus the persistence length in units of the total length of the polymer. The curves are parameterized by the relative angle  $\theta_0$  of the force  $\mathbf{f}$  to the initial orientation.

method is well suited to investigate also more complex questions concerning for example the interactions with actin binding proteins which among others can induce cross-linking or bundling.

In order to describe the material properties of the cytoskeleton, one has to understand how semiflexible polymers built up statistical networks and how the macroscopic stresses and strains are mediated to the single filaments in such a “rigid polymer network”. This is a quite rapidly growing field in polymer physics with many questions still open (Aharoni and Edwards, 1994).

If the polymers are not crosslinked, the response will depend on how fast one pulls. Roughly speaking, the solution will either show elastic behavior and obey Hook’s law with a linear relation  $\sigma = G\gamma$  between stress  $\sigma$  and strain  $\gamma$  or rather show viscous behavior and obey Newton’s law  $\sigma = \eta\dot{\gamma}$ , where the stress is proportional to the strain rate  $\dot{\gamma}$ . The task of a theoretical description is to find out how the material parameters like the shear modulus  $G^0$  and the viscosity  $\eta$  depend on the elastic and dynamic properties of the polymers and the architecture of the network. The mechanical and dynamical properties of the various crosslinking proteins are also expected

to influence the viscoelasticity of the network (Wachsstock et al., 1994).

Whereas it is known that on short time scales the effect of mutual steric hindrance (“entanglement”) in conventional polymeric materials is very similar to the effect of permanent chemical crosslinks, this is an open problem for semiflexible polymer networks. Since forces between neighboring polymers can only be transmitted transverse to the polymer axis and there is no restoring force for sliding of one filament past another, a steric contact is acting completely different from a chemical crosslink on a microscopic scale.

But even the most simple of these problems, the static elasticity of a network of permanently crosslinked semiflexible polymers, is quite complex. Because of the strongly anisotropic behavior of the single elements, the predicted macroscopic properties of the network vary greatly with the explicit or implicit assumptions made about network geometry and stress propagation by recent theoretical treatments of both entangled solutions and crosslinked networks (MacKintosh et al., 1995; Isambert and Maggs, 1996; Satcher and Dewey, 1996; Kroy and Frey, 1996). We hope to represent a key aspect of the geometrical structure of both cellular and artificial stiff polymer networks by looking at *disordered* networks. Specifically, we use a crosslinked network of sticks randomly placed in a plane as a toy model for studying the origin of macroscopic elasticity in a stiff polymer network. Although quantitative predictions about the behavior of existing (three-dimensional) networks of semiflexible polymers are not attempted at this stage, this model is expected to reflect the salient features of the full problem and to promote its understanding by allowing the detailed discussion of questions like “What modes of deformation contribute most to the network elasticity?”, “How many filaments do actually carry stress, how many remain mostly unstressed?”, “What kind of effective description of the complicated microscopic network geometry should be used?”. This approach connects the theory of cytoskeletal elasticity to the very active fields of transport in random media and elastic percolation. In section 3.4 we will describe the model in more detail and discuss the question of the dominant deformation mode.

Previous fluorescence microscopic observations (Käs et al., 1994) suggest that the tube picture is a useful concept for understanding the viscoelastic properties of *entangled* semiflexible polymer networks. Starting from this model, where the matrix surrounding a single test polymer is represented by a tube-like cage, we have developed a phenomenological description that seems to be able to account for some of the observed elastic and dynamic properties. The predictions for the entanglement transition, the concentration dependence of the plateau modulus, and the terminal relaxation time are in good quantitative agreement with experimental data.

## 2 Single-chain properties

## 2.1 The wormlike chain model

The theoretical understanding of the mechanical properties of a *single* semiflexible macromolecule in isolation is already a nontrivial statistical mechanics problem with quite a number of recent developments 50 years after it was first formulated (Kratky and Porod, 1949). The model usually adopted for a theoretical description of semiflexible chains like actin filaments is the *wormlike chain model*. The filament is represented by an inextensible space curve  $\mathbf{r}(s)$  of total length  $L$  parameterized in terms of the arc length  $s$ . The statistical properties of the wormlike chain are determined by a free energy functional which measures the total elastic energy of a particular conformation.

$$\mathcal{H} = \int_0^L ds \frac{\kappa}{2} \left( \frac{\partial \mathbf{t}}{\partial s} \right)^2 ; \quad |\mathbf{t}| = 1, \quad (1)$$

where  $\mathbf{t}(s) = \partial \mathbf{r}(s) / \partial s$  is the tangent vector. The energy functional is quadratic in the local curvature with  $\kappa$  being the bending stiffness of the chain. The inextensibility of the chain is expressed by the local constraint,  $|\mathbf{t}(s)| = 1$ , which leads to non-Gaussian path integrals. Since there would be high energetic costs for a chain to fold back onto itself one may safely neglect self-avoidance effects for sufficiently stiff chains.

Despite the mathematical difficulty of the model some quantities can be calculated exactly. Among these is the tangent-tangent correlation function which decays exponentially,  $\langle \mathbf{t}(s) \cdot \mathbf{t}(s') \rangle = \exp[-(s - s') / \ell_p]$ , with the persistence length  $\ell_p = \kappa / k_B T$  (in three dimensional space). Another example is the mean-square end-to-end distance

$$\begin{aligned} \mathcal{R}^2 &:= \langle R^2 \rangle = 2\ell_p^2 (e^{-L/\ell_p} - 1 + L/\ell_p) \\ &= \begin{cases} L^2 & \text{for } L/\ell_p \rightarrow 0 \text{ (rigid rod)} \\ 2\ell_p L & \text{for } L/\ell_p \rightarrow \infty \text{ (random coil)}, \end{cases} \end{aligned} \quad (2)$$

which reduces to the appropriate limits of a rigid rod and a random coil (with Kuhn length  $2\ell_p$ ) as the ratio of  $L$  to  $\ell_p$  tends to zero or infinity, respectively. The calculation of higher moments quickly gets very troublesome (Hermans and Ullman, 1952).

## 2.2 Linear force-extension relation

Another useful property of the model, which can be computed exactly is the linear force extension relation (Kroy and Frey, 1996). Adding a term  $-\mathbf{f} \cdot \mathbf{R}$  to the Hamiltonian in Eq. 1, the extension of a wormlike chain with a weak force applied between its ends is computed as

$$\delta R = (\langle \mathbf{R} \rangle_f - \langle \mathbf{R} \rangle_0) \mathbf{f} / f = f(\mathcal{R}^2 - \langle |\mathbf{R}| \rangle^2) / k_b T = f/k \quad (3)$$

with  $k$  the force coefficient. The problem is the calculation of the moment of the the end-to-end distance  $\langle |\mathbf{R}| \rangle$ . This has not been achieved so far, but an expansion in the stiff limit is possible. For example, we can write  $\langle |\mathbf{R}| \rangle = \mathcal{R} \langle \sqrt{1 + (R^2 - \mathcal{R}^2)/\mathcal{R}^2} \rangle$  and expand the square root to obtain to leading order for the force coefficient

$$4k_B T \frac{\mathcal{R}^2}{\langle R^4 \rangle - \mathcal{R}^4} \xrightarrow{L/\ell_p \ll 1} \frac{90\kappa^2}{k_B T L^4}.$$

This is exact in the stiff limit,  $L/\ell_p \ll 1$ , and qualitatively correct over the whole range of stiffness. However, for the special boundary condition of a grafted chain we can even get an *exact result for arbitrary stiffness*. Consider a chain with one end clamped at a fixed orientation and let us apply a force at the other end. Then the linear response of the chain may be characterized in terms of an effective Hookian spring constant which depends on the orientation  $\theta_0$  of the force with respect to the tangent vector at the clamped end. In the appropriate generalization of the second part of Eq. 3 the force coefficient  $k$  is replaced by an angle dependent function,  $k^{-1} \rightarrow L^2 \mathcal{F}_{\theta_0}(\ell_p/L)/k_B T$ . Noting that the conformational statistics of the wormlike chain is equivalent to the diffusion on the unit sphere (Saitô et al., 1967) the function  $\mathcal{F}$  can be calculated (Kroy and Frey, 1996) (see Fig. 1). In the flexible limit, where the chain becomes an isotropic random coil, all curves coincide and reproduce entropy elasticity,  $\mathcal{F}_{\theta_0}(x) \sim x$ . But for stiff chains the force-extension relation depends strongly on the value of the angle  $\theta_0$  between the force and the grafted end. Transverse forces give rise to ordinary mechanical bending characterized by the bending modulus  $\kappa$  ( $\mathcal{F}_{\pi/2} \sim 1/x$ ), whereas longitudinal deformations are resisted by a larger force coefficient  $\kappa^2/T$  ( $\mathcal{F}_0 \sim 1/x^2$ ). The breakdown of linear response in the limit  $T \rightarrow 0$  (or  $\ell_p \rightarrow \infty$ ) is a consequence of the well known Euler buckling instability, as we already mentioned in the introduction. The linear response for longitudinal forces is due to the presence of thermal undulations, which tilt parts of the polymer contour with respect to the force direction.

### 2.3 Nonlinear Response and radial distribution function

In viscoelastic measurements on *in vitro* actin networks one observes strain hardening (Janmey et al., 1990), i.e. the system stiffens with increasing strain. This may either result from collective nonlinear effects or from the nonlinear response of the individual filaments. In the preceding section we have seen that the force coefficient obtained in linear response analysis for longitudinal deformation diverges in the limit of vanishing thermal fluctuations indicating that the regime of validity for linear response shrinks with increasing stiffness. Since the nonlinear response of a single filament may be obtained from the radial distribution function by integration, we discuss the latter first.

A central quantity for characterizing the conformations of polymers is the radial distribution function  $G(\mathbf{R}; L)$  of the end-to-end vector  $\mathbf{R}$ . For a freely jointed phantom chain (flexible polymer) it is known exactly and for many purposes well approximated by a simple Gaussian distribution. While rather flexible polymers can be described by corrections to the Gaussian behavior (Daniels, 1952), the distribution function of polymers which are shorter or comparable to their persistence length shows very different behavior. It is in good approximation given by

$$G(\mathbf{R}; L) \approx \frac{\ell_p}{\mathcal{N}L^2} f\left(\frac{\ell_p}{L}(1 - R/L)\right),$$

$$\text{where } f(x) = \begin{cases} \frac{\pi}{2} \exp[-\pi^2 x] & \text{for } x > 0.2 \\ \frac{1/x - 2}{8\pi^{3/2} x^{3/2}} \exp\left[-\frac{1}{4x}\right] & \text{for } x \leq 0.2 \end{cases} \quad (4)$$

and  $\mathcal{N}$  is a normalization factor close to 1 (Wilhelm and Frey, 1996). This result is valid for  $L \lesssim 2\ell_p$ ,  $x \lesssim 0.5$  and  $d = 3$  where  $d$  is the dimension of space. A similar expression exists for  $d = 2$ . As can be seen in Fig. 2, the maximum weight of the distribution shifts towards full stretching as the stiffness of the chain is increased to finally approach the  $\delta$ -distribution like shape required for the rigid rod.

The radial distribution function is a quantity directly accessible to experiment since fluorescence microscopy has made it possible to observe the configurations of thermally fluctuating biopolymers (Gittes et al., 1993; Käs et al., 1993; Ott et al., 1993). Comparing the observed distribution functions with the theoretical prediction for  $d = 2$  is both a test of the validity of the wormlike chain model for actual biopolymers as well as a sensitive method to determine the persistence length which is the only fit parameter. It should be noted here that the determination of persistence length e.g. of actin is still an actively discussed subject (Dupuis et al., 1996; Wiggins et al., 1997).

A very interesting possibility would be to attach two or more markers (e.g., small fluorescent beads) permanently to single strands of polymers and to observe the distribution function of the marker separation. This would eliminate all the experimental difficulties associated with the determination of the polymer contour. Note that in contrast to existing methods of analysis it is not necessary to know the length of polymer between two markers; it can be extracted from the observed distribution functions along with  $\ell_p$  by introducing  $L$  as a second fit parameter.

The nonlinear response of the polymer to extending or compressing forces can be obtained from the radial distribution function by integration. The result (Fig. 2) is in agreement with and provides the transition between the previously known limits of linear response and very strong extending forces (e.g., (Marko and Siggia, 1995)). For compressional forces, a pronounced de-

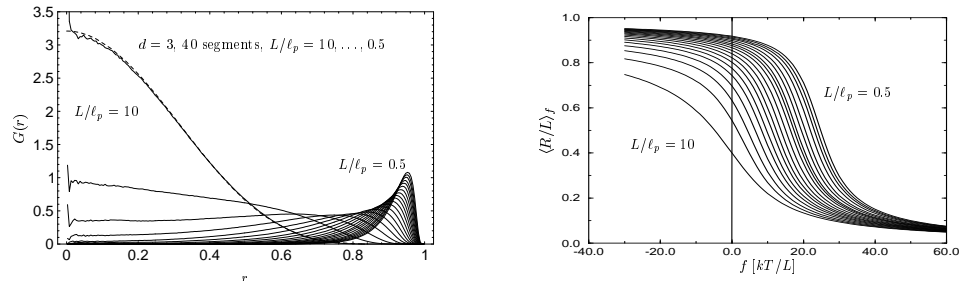


Figure 2: *Left:* End-to-end distribution function of a semiflexible polymer (numerical results). Note that with increasing stiffness of the polymer there is a pronounced crossover from a Gaussian to a completely non-Gaussian from with the weight of the distribution shifting towards full stretching. *Right:* The mean end-to-end distance  $R$  as a function of a force applied between the ends ( $\mathbf{f} = -f\mathbf{R}/|\mathbf{R}|$ ). The step at positive (i.e. compressive) forces can be viewed as a remnant of the Euler instability.

crease of differential stiffness around the classical critical force  $f_c = \kappa\pi^2/L^2$  can be understood as a remnant of the Euler instability. For filaments slightly shorter than their persistence length the influence of this instability region extends up to and beyond the point of zero force corresponding to the maximum in the linear response coefficient for  $\ell_p \approx L$  (see Fig. 1). For large compressions beyond the instability, the force-extension-relation calculated from the distribution function is only in qualitative agreement with numerical results because of the restricted validity of Eq. 4 for  $x \rightarrow 1$ .

## 2.4 Dynamic structure factor

The short time dynamics of polymers is most effectively measured by scattering techniques. The *dynamic structure factor* of a semiflexible polymers can be derived analytically in the limit of strong length scale separation  $a \ll \lambda \ll \ell_p, L$  ('weakly bending rod' approximation) and  $\lambda \leq \xi_m$ . Here we have introduced the symbols  $a$ ,  $\lambda$  and  $\xi_m$  for the lateral diameter of the polymer, the scattering wavelength and the mesh size of the network, respectively. The length scale separation guarantees that the decay of the structure factor is due to the *internal dynamics of single filaments*. For  $\lambda \approx \xi_m$  the structure factor decays in two steps due to the fast internal and to the slower collective modes, respectively. For the analysis we will restrict ourselves to rather dilute solutions and refer the reader for a more complete treatment to the literature (Kroy and Frey, 1997).

The most important result of the calculations is that the time decay of the dynamic structure factor shows two regimes: the simple exponential

initial decay regime for  $t \ll \tau = \tilde{\zeta}_\perp / \kappa k^4$  with a decay rate

$$\gamma_k^{(0)} = \frac{k_B T}{6\pi^2 \eta} k^3 \left( \frac{5}{6} - \ln ka \right), \quad (5)$$

and the stretched exponential decay

$$g(\mathbf{k}, t) \propto \exp \left( -\frac{\Gamma(\frac{1}{4})}{3\pi} (\gamma_k t)^{\frac{3}{4}} \right), \quad \gamma_k = k_B T k^{\frac{8}{3}} / \ell_p^{1/3} \tilde{\zeta}_\perp \quad (6)$$

for  $t \gg \tau$ . The effective transversal friction coefficient per length,  $\tilde{\zeta}_\perp$ , ac-

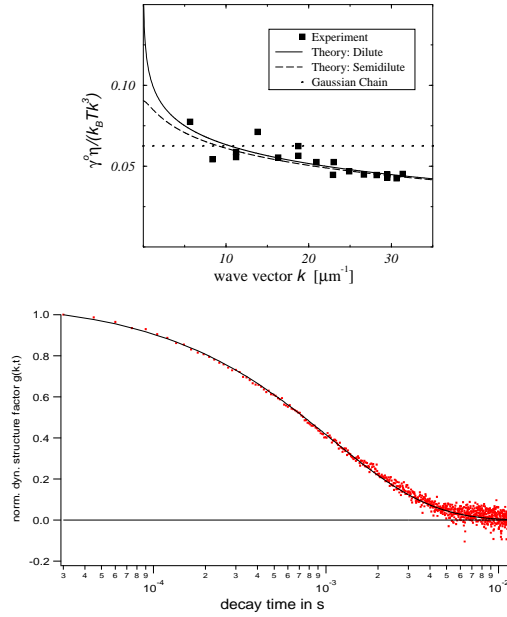


Figure 3: Results from dynamic light scattering experiments. *Left*: Correction to the classical prediction  $\gamma_k^{(0)} \sim k^3$  for the initial decay rate of the dynamic structure factor. The theoretical predictions for dilute solutions (solid line) and semidilute solutions (dashed line) are compared with experimental data (Schmidt et al., 1989). Also included is the prediction for Gaussian chains from Ref. (Doi and Edwards, 1986). *Right*: Fit of theoretical dynamic structure factor to experimental data for  $k = 24.2 \mu\text{m}^{-1}$  (Götter et al., 1996).

counts for the hydrodynamic damping of the undulations on length scales comparable to the scattering wavelength. For polymers with  $\ell_p \approx \lambda$  mainly the first regime, Eq. 5, is observed. The microscopic lateral diameter  $a$  of

the polymer enters the calculation as a microscopic cutoff and can be determined from a measurement of the *initial decay* of the dynamic structure factor. The method is easy to apply and has been shown to provide reasonably accurate results (see Fig. 3). For polymers with  $\ell_p \gg \lambda$  mainly the stretched exponential decay regime, Eq. 6 is observed. The decay rate is determined by the persistence length of the molecule, which is also readily extracted from experimental data. Some applications of the methods to dynamic light scattering with actin are shown in Fig. 3.

Our analytical results for the initial decay rate and the dynamic exponent for semiflexible polymers suggest that known deviations of the dynamic exponent for more flexible polymers from its classical value  $z = 3$  are most likely due to the local semiflexible structure of these molecules, and that the above analysis is therefore of some relevance also to scattering from flexible polymers. The reason is that the singular ( $\propto 1/r$ ) hydrodynamic interaction favors short distances. The possibility to determine the microscopic lateral diameter  $a$  of the polymer from the initial decay becomes important when the effects of bundling and side-binding are investigated, which can give rise to an effective thickening of the molecules.

### 3 Many-chain properties

As we have mentioned in the introduction, we are still far from understanding on a microscopic basis the macroscopic viscoelastic properties of solutions and gels of semiflexible polymers. In the following we will review some idealized concepts we have developed to model certain aspects of this complicated behavior and compare our predictions with some recent experiments.

#### 3.1 Entanglement transition

Upon increasing the polymer concentration  $c$  at fixed polymer length there is a critical concentration  $c^*$  above which a plateau develops in the frequency dependence of the storage modulus and the modulus increases steeply. The same phenomenon is observed at a critical length when the polymer length is varied at fixed concentration. It is called the entanglement transition. An experimental observation of the transition for short actin filaments ( $L \approx 1.5 \mu\text{m}$ ) as a function of concentration is shown in Fig. 4 (left). Adapting concepts which have been developed for flexible polymers (Kavassalis and Noolandi, 1989) we have proposed a mean field description for the entanglement transition in semiflexible polymer solutions (Kroy and Frey, 1996). The basic idea is that the ends of a polymer are less efficient in confining other polymers than internal parts of the polymer. As a consequence the critical concentration  $c^*$  is related to the overlap concentration  $\bar{c}$  by some universal number  $C$  which may be interpreted as an effective coordination

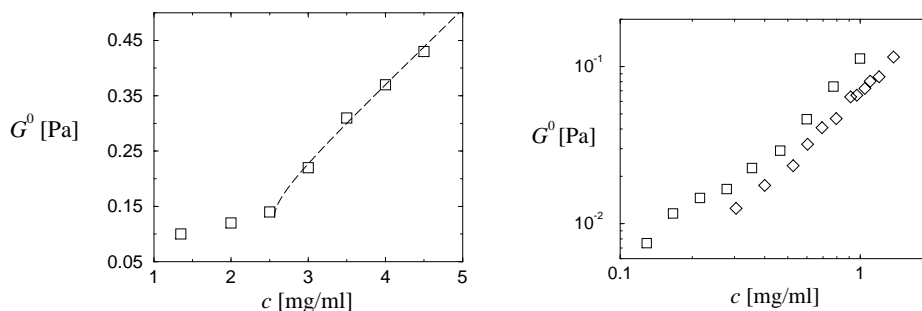


Figure 4: *Left:* The entanglement transition for short rod-like actin filaments ( $L \approx 1.5 \mu\text{m}$ ) of varying concentration. *Right:* Concentration dependence of the plateau modulus for pure actin ( $\square$ ) and actin with a small amount of gelsolin ( $\diamond$ ) (Hinner et al., 1997).

number and is a measure of the mean number of neighboring polymers necessary to confine the lateral motion of the test polymer. The prediction for an ideal gas of rods,  $G^0 \propto k_B T / \xi_{\text{eff}}^2 L$ , is also shown in Fig. 4. From the fit we have determined the coordination number  $C$ , which compares very well with the result for flexible polymer solutions. Away from the transition the effective mesh size reduces to the ordinary mesh size  $\xi_{\text{eff}} \propto \xi_m$ . With  $\xi_m \propto c^{-1/2}$  (Schmidt et al., 1989) this implies  $G^0 \propto c$ , which is indeed observed for a regime of concentrations within the semidilute phase. However, at higher concentrations or lengths the slope of  $G^0(c)$  increases, as can be seen from the bottom plot in Fig. 4, which shows the measured plateau modulus  $G^0$  for pure actin and actin with a small amount of gelsolin ( $r_{\text{AG}} = 6000 : 1$  corresponding to an average actin filament length of  $16 \mu\text{m}$ ). The description of the polymers as rods, which neglects internal modes of the individual polymers, is no longer appropriate. NOTE: Since the time of writing this manuscript, new experimental and theoretical investigations (Hinner et al., 1997) have suggested another, probably superior, interpretation of the entanglement transition, which does not involve the concept of the coordination number.

### 3.2 Plateau modulus

To explain the observed elastic modulus on the basis of the elastic properties of the individual chains and the architecture of the network is in general a quite difficult task. Some of the theoretical work is based on a tube picture as depicted schematically in Fig. 5. The effect of the network surrounding an arbitrary test polymer is represented by a cylindrical cage of diameter  $d$ . The main response of the polymer to various deformations of this tube

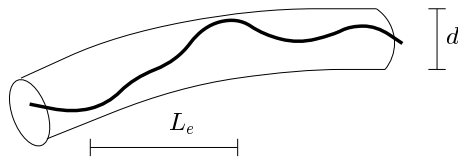


Figure 5: Some of the theoretical work is based on a tube picture as depicted schematically here. The effect of the network surrounding an arbitrary test polymer is represented by a cylindrical cage of diameter  $d$ . Different scaling laws for  $d$  have been proposed.

is assumed to arise from distortions of undulations of wavelength  $L_e$ , with  $L_e^3 \propto d^2 \ell_p$  (Odijk, 1983). It is far from obvious, whether the macroscopic elasticity can be explained solely in terms of the compressibility of the tubes (Odijk, 1983; Isambert and Maggs, 1996), or whether contributions from filament bending (Kroy and Frey, 1996; Satcher and Dewey, 1996) or buckling (MacKintosh et al., 1995) are also important. The theoretical approaches differ quite significantly in their assumptions on how forces are transmitted through the network and which type of deformation of a single polymer gives the dominant contribution to the network elasticity. Due to those differences in the basic assumptions the predictions for the shear modulus of the network also differ. Our present data are reasonably consistent with entropy arguments assuming  $G^0 \propto k_B T / \xi_m^2 L_e$ , which leads to  $G^0 \propto c^{4/3}$  for  $d \propto \xi_m$  and  $G^0 \propto c^{7/5}$  for  $d \propto \xi_m^{5/6} / \ell_p^{1/5}$  (Isambert and Maggs, 1996), respectively. Above 0.4 mg/ml our data also agree with a scaling  $G^0 \propto c^{5/3}$ , which has been derived by a scaling argument based on Fig. 5 for the case that the macroscopic elastic response is mainly due to filament bending (Kroy and Frey, 1996). It should also be noted that these concentrations are close to the critical volume fraction  $3a/L$  ( $a \approx 10$  nm is the lateral diameter of an actin filament) for the nematic transition of rigid rods.

### 3.3 Terminal relaxation

At frequencies below the plateau regime the elastic response decreases and the polymer solution starts to flow. The corresponding time scale is called the terminal relaxation time. It can be determined from the measured plateau modulus and the zero shear rate viscosity using the relation  $\eta_0 \sim G^0 \tau_r$  or directly from  $G'(\omega)$ .

Intuitively, the mechanism for the terminal relaxation is obvious from the tube picture (see Fig. 6) described above: viscous relaxation only occurs, when the polymers have time to leave their tube-like cages by reptation, i.e., by Brownian motion along their axis. The reptation model, which was originally formulated for flexible polymers, was adapted to the semiflexible

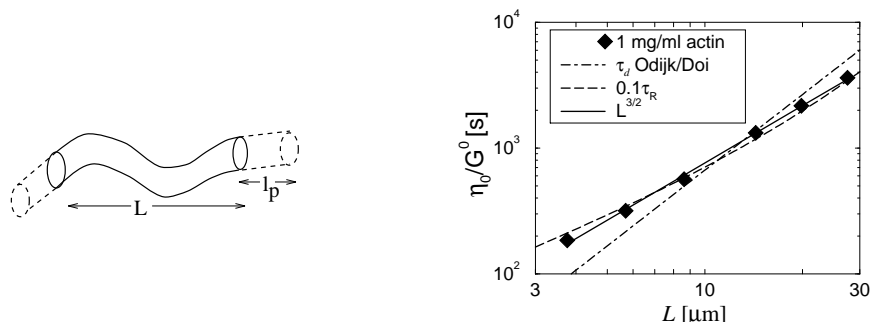


Figure 6: *Left:* Illustration of the generalized reptation picture for semiflexible polymer solutions. *Right:* Terminal relaxation time above the entanglement transition (Hinner et al., 1997).

case (Odijk, 1983). Odijk (Odijk, 1983) estimated the disengagement time  $\tau_d$  for a semiflexible chain diffusing out of its tube. However, the data for  $\tau_r$  presented in Fig. 6 (bottom) are not in accord with his result for  $\tau_d$ . The dependence of the observed terminal relaxation time  $\tau_r$  on polymer length  $L$  is substantially weaker than predicted for  $\tau_d$ , even in the stiff limit where  $\tau_d = \ell_p L / 4D_{\parallel} \propto L^2$  (dot-dashed line in Fig. 6),  $D_{\parallel} = k_B T / 2\pi\eta L$  being the longitudinal diffusion coefficient of the chain in the free draining approximation. Instead, the solid line in Fig. 6 corresponds to the scaling law  $\tau_r \propto L^{3/2}$ .

A tentative interpretation of the data can be given in terms of a semiflexible polymer diffusing along a strictly one dimensional path; i.e., not being allowed to choose between infinitely many new directions at its ends. This situation is schematically depicted in the upper part of Fig. 6. The characteristic decay time for self-correlations of the end-to-end vector  $\langle \mathbf{R}(t)\mathbf{R} \rangle$  is then given by (Hinner et al., 1997)

$$\tau_R = L^4 \ell_p^2 / D_{\parallel} \langle R^2 \rangle^2 \approx (L + 2\ell_p)^2 / 4D_{\parallel}. \quad (7)$$

This presents an upper bound for the terminal relaxation time within the tube model. As seen from the dashed line in Fig. 6,  $\tau_R$  (for  $\ell_p = 17 \mu\text{m}$  (Gittes et al., 1993; Ott et al., 1993)) is in fact by a factor of ten too large compared to the data but describes fairly well the length dependence of  $\tau_r$ . The restriction to one path implies a very slow decay of conformational correlations. An unusually slow decay of stress (the frequency dependence of  $G'(\omega)$  is still less than linear in the measured frequency range) is indeed observed, but this might also in part be due to the broad length distribution of actin (Janmey et al., 1986). Clearly, further investigations are necessary to come to a better understanding of the terminal regime.

### 3.4 Stochastic network models

As motivated in the introduction, we use a two dimensional toy model of crosslinked semiflexible polymer networks to study some of the fundamental problems in semiflexible network theory (Wilhelm and Frey, 1998). Here we address the question whether longitudinal or transversal deformation dominate the network response and find an interesting crossover between the two extreme cases. Since such questions are already nontrivial for networks at  $T = 0$  (i.e. no fluctuations), we consider this most simple case first: The linear elastic response of a network of classical compressible and bendable rods. A more sophisticated treatment will include contour fluctuations of the filaments (but no steric interactions) by replacing the rods with elements having the appropriate linear or nonlinear force extension relations described above.

Rods of unit length are randomly placed on a square piece of the plane. Wherever two sticks intersect, they are connected by a crosslink. Periodic boundary conditions are applied to the left and right sides of the square. A shearing horizontal displacement is enforced on all rods intersecting the upper or lower boundary of the square at the intersection points. The (linearized) elastic equations of the system are solved numerically for displacements and forces at all crosslink points. The shear modulus is obtained from the force needed to impose the displacements of the upper and lower boundary. Crosslinks are not allowed to stretch but do not fix the angle between the intersecting rods. The results reported here change quantitatively but not qualitatively when crosslinks do fix the intersection angles.

The parameters of this system are the density  $\rho$  of rods per unit area, the compressional and the bending stiffness of the rods. We choose to express the latter by the linear response force constants  $k_{\text{comp}}$  and  $k_{\text{bend}}$  for a rod of unit length. Geometrically, the relative size of the two force constants is controlled by the aspect ratio  $\alpha = a/L$  of the rods where  $a$  is the rod radius.

While the system can show no elastic response (in the limit of infinite size) for densities below the percolation threshold  $\rho_c^g \approx 5.72$  (Pike and Seager, 1974), the shear modulus  $G$  grows very rapidly with increasing  $\rho$  for  $\rho \geq \rho_c$ . For sufficiently slender rods  $G$  displays unusual power law behavior in  $\rho$  even for densities far above the percolation threshold.

To address the question whether the elasticity of a random stiff polymer network is dominated by transverse or by longitudinal deformations of the filaments, one can study the dependence of the shear modulus on the two force constants. We keep  $k_{\text{bend}}$  fixed and increase  $k_{\text{comp}}$  from values corresponding to  $\alpha = 0.15$  (short, thick rod) to values corresponding to  $\alpha = 1 \times 10^{-5}$  (long slender rod) for different system densities (see Fig. 7). We observe that beyond a certain point the shear modulus ceases to depend on  $k_{\text{comp}}$ , indicating that the elasticity is dominated by bending modes for

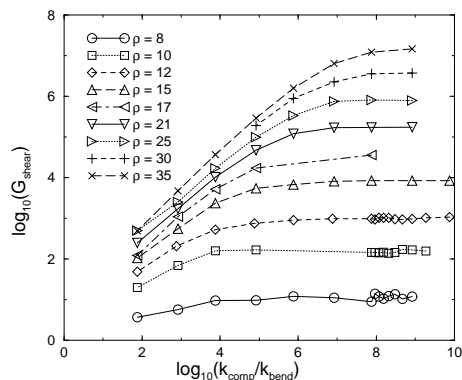


Figure 7: Shear modulus of a crosslinked two dimensional random network of rods of unit length for different densities  $\rho$  and different aspect ratios  $\alpha$  plotted over the relative size  $k_{\text{comp}}/k_{\text{bend}}$  of compressional and bending force constants. Units were chosen in such a way that the bending stiffness  $\kappa$  and hence  $k_{\text{bend}}$  were constant ( $\kappa = 1$ ).

thin rods. Since the relevant scale for the system elasticity at higher densities is set not by the rod length but by the mesh size, the point of onset for this behavior shifts upwards with density. The dominance of bending modes in this region is confirmed by the observation that almost all of the energy stored in the deformed network is accounted for by the transverse deformation of the rods. Even in the region where the shear modulus does depend on  $k_{\text{comp}}$ , a substantial part of the elastic energy is stored in bending deformations.

**Acknowledgment:** Our work has been supported by the Deutsche Forschungsgemeinschaft (DFG) under Contract No. SFB 266 and No. Fr 850/2.

## References

- Aharoni, S. M. and S. F. Edwards. 1994. *Rigid Polymer Networks*, volume 118 of *Advances in Polymer Science*. Springer, Berlin.
- Daniels, H. E. 1952. *Proc. Roy. Soc. Edinburgh*, 63A:290.
- Doi, M. and S. F. Edwards. 1986. *The Theory of Polymer Dynamics*. Clarendon Press, Oxford.
- Dupuis, D. E., W. H. Guiford, and D. M. Warshaw. 1996. *Biophys. J.*, 70:A268.
- Eichinger, L., B. Köppel, A. Noegel, M. Schleicher, M. Schliwa, K. Weijer, W. Witke, and P. Janmey. 1996. *Biophys. J.*, 70:1054.
- Farge, E. and A. C. Maggs. 1993. *Macromol.*, 26:5041.
- Gittes, F. *et al.* 1993. *Journal of Cell Biology*, 120:923.

- Götter, R., K. Kroy, E. Frey, M. Bärmann, and E. Sackmann. 1996. *Macromol.*, 29:30.
- Harnau, L., R. G. Winkler, and P. Reineker. 1996. *J. Chem. Phys.*, 140:6355.
- Hermans, J. J. and R. Ullman. 1952. *Physica*, 44:2595.
- Hinner, B., M. Tempel, E. Sackmann, K. Kroy, and E. Frey. 1997. *cond-mat/9712037*.
- Isambert, H. and A. C. Maggs. 1996. *Macromol.*, 29:1036.
- Janmey, P. 1995. *Cell Membranes and the Cytoskeleton*, volume 1A of *Handbook of biological physics*, chapter 17, page 805. North Holland, Amsterdam.
- Janmey, P. A. 1991. *Curr. Op. Cell. Biol.*, 2:4.
- Janmey, P. A., S. Hvidt, F. George, J. Lamb, and T. Stossel. 1990. *Nature*, 347:95.
- Janmey, P. A., J. Peetermans, K. S. Zaner, T. P. Stossel, and T. Tanaka. 1986. *J. Biol. Chem.*, 261:8357.
- Käs *et al.*. 1993. *Europhysics Letters*, 21:865.
- Käs, J., H. Strey, and E. Sackmann. 1994. *Nature*, 368:226.
- Kavassalis, T. A. and J. Noolandi. 1989. *Macromol.*, 22:2709.
- Kratky, O. and G. Porod. 1949. *Rec. Trav. Chim.*, 68:1106.
- Kroy, K. and E. Frey. 1996. *Phys. Rev. Lett.*, 77:306.
- Kroy, K. and E. Frey. 1997. *Phys. Rev. E*, 55:3092.
- MacKintosh, F., J. Käs, and P. Janmey. 1995. *Phys. Rev. Lett.*, 75:4425.
- Marko, J. F. and E. D. Siggia. 1995. *Macromol.*, 28:8759.
- Odijk, T. 1983. *Macromol.*, 16:1340.
- Ott, A., M. Magnasco, A. Simon, and A. Libchaber. 1993. *Phys. Rev. E*, 48:R1642.
- Pike, G. E. and C. H. Seager. 1974. *Phys. Rev. B*, 10:1421.
- Saitô, N., K. Takahashi, and Y. Yunoki. 1967. *J. Phys. Soc. Jap.*, 22:219.
- Satcher, Jr., R. L. and C. F. Dewey, Jr. 1996. *Biophys. J.*, 71:109–118.
- Schmidt, C., M. Bärmann, G. Isenberg, and E. Sackmann. 1989. *Macromol.*, 22:3638.
- Wachsstock, D., W. Schwarz, and T. Pollard. 1994. *Biophys. J.*, 66:801.
- Wiggins, C. H., D. X. Riveline, A. Ott, and R. E. Goldstein. 1997. Trapping and wiggling: Elastohydrodynamics of driven microfilaments. *cond-mat/9703244*.
- Wilhelm, J. and E. Frey. 1996. *Phys. Rev. Lett.*, 77:2581.
- Wilhelm, J. and E. Frey. 1998. Elasticity of stiff polymer networks. in preparation.